Universal Unitary Transfer of Continuous-Variable Quantum States into a Few Qubits

Jacob Hastrup,[1,*] Kimin Park,[2,1] Jonatan Bohr Brask,[1] Radim Filip,[2] and Ulrik Lund Andersen[1]
[1]Center for Macroscopic Quantum States (bigQ), Department of Physics, Technical University of Denmark, 2800 Kongens Lyngby, Denmark
[2]Department of Optics, Palacky Univeristy, 77146 Olomouc, Czech Republic

(Received 23 June 2021; accepted 14 February 2022; published 15 March 2022)

We present a protocol for transferring arbitrary continuous-variable quantum states into a few discrete-variable qubits and back. The protocol is deterministic and utilizes only two-mode Rabi-type interactions that are readily available in trapped-ion and superconducting circuit platforms. The inevitable errors caused by transferring an infinite-dimensional state into a finite-dimensional register are suppressed exponentially with the number of qubits. Furthermore, the encoded states exhibit robustness against noise, such as dephasing and amplitude damping, acting on the qubits. Our protocol thus provides a powerful and flexible tool for discrete-continuous hybrid quantum systems.

DOI: 10.1103/PhysRevLett.128.110503

Introduction.—Quantum information processing (QIP) can be realized using both discrete variables (DV), such as the energy levels of atoms or superconducting qubits, or continuous variables (CV) [1], such as the quadratures of an electromagnetic field, spin ensemble, or mechanical oscillator. Both types of systems have various advantages and disadvantages, depending on the particular task, application, and implementation. For example, universal control of noisy many-qubit systems has become available [2], but truly scalable systems and breakeven error correction remains to be demonstrated. On the other hand, CV QIP is highly scalable, allowing long range interactions that have been used to demonstrate entanglement of millions of modes [3] and generation of 2D cluster states [4,5] with current technology. Furthermore, the infinite dimensionality of a single CV mode can be utilized for hardware-efficient single-mode error correction [6–9], and high-dimensional operations, such as the quantum Fourier transform, can be implemented with simple single-mode operations [1]. However, non-Gaussian operations required for universal quantum processing and fault tolerance have proven difficult to realize in pure CV systems.

Two of the leading platforms for quantum computing are trapped ions and superconducting circuits. These systems support both DV QIP through spin or charge qubits, as well as CV QIP through motional modes or microwave cavity modes. Furthermore, the CV and DV modes can couple, enabling CV-DV hybrid interactions. In fact, it is common to utilize this hybrid interaction to enable various operations. For example, for DV QIP, the CV modes can be used to facilitate multimode operations and qubit readout [10,11]. Meanwhile, for CV QIP, the DV modes are used to enable non-Gaussian operations [6–9] that are required for universality. Thus, CV-DV hybrid interactions have proven valuable in overcoming the challenges associated with either CV or DV QIP.

Here, we add a new element to the toolbox of CV-DV hybrid operations by showing that arbitrary quantum states can be coherently and deterministically mapped between a CV mode and a collection of qubits using accessible two-mode interactions. This mapping has several potential applications for QIP. For example, our scheme enables qubit-based memories for CV states. Many types of CV QIP rely on heralded, nondeterministic operations and are therefore dependent on quantum memories. A qubit-based memory could enable DV error correction protocols to be carried out on arbitrary CV states. Additionally, if the qubits are coupled to two different CV modes, e.g., transmon qubits coupled to both a mechanical acoustic mode and a microwave cavity mode, one CV mode can be encoded to the qubits and then decoded onto the other CV mode, enabling qubit-mediated transfer of CV information from one CV mode to another. Furthermore, our scheme can also be used for efficient deterministic generation of arbitrary CV states, such as non-Gaussian states, by preparing the qubits in an equivalent encoded state and then applying the inverse mapping to transfer the state to the CV mode. In general, applications of this protocol will strongly depend on the physical system but promise to aid in solving a wide range of issues in hybrid QIP platforms.

Protocols for transferring CV states into qubits have previously been proposed [12,13]. However, unlike Ref. [12] our protocol makes efficient use of the available qubit dimensionality, such that only a few qubits are required, and unlike Ref. [13] our protocol uses only experimentally available interactions.

Protocol.—The system we are considering consists of a single CV mode and $N > 1$ qubits, as illustrated in Fig. 1(a). The protocol is designed to transfer an arbitrary CV state $|\psi\rangle_{\mathrm{CV}}$ into an entangled state of the qubits, leaving the CV mode in an input-independent state, which we denote $|\tilde{0}\rangle_{\mathrm{CV}}$.

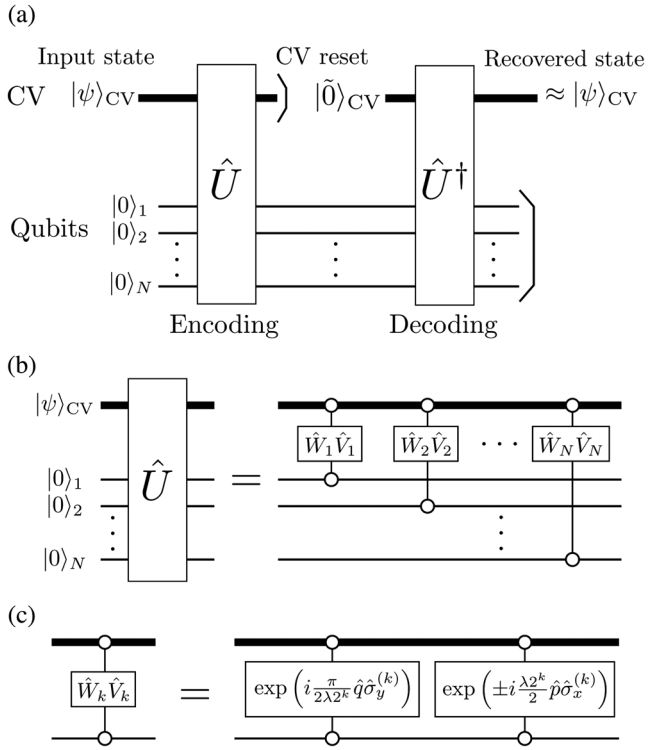

FIG. 1. (a) Circuit of encoding and decoding to transfer a CV state to a collection of qubits and back. (b) The encoding is achieved by interacting the CV mode sequentially with each of the qubits. (c) Each interaction unitary is composed of two Rabi interactions as given by Eq. (3).

Since the CV mode has an infinite dimensionality while the qubits have a finite dimension, such a protocol is in principle impossible for arbitrary states. However, in practice we can expect relevant input CV states to have majority of their support in a finite-dimensional subspace, thereby allowing a CV-DV mapping to a good approximation. Furthermore, since the dimension of the qubit subspace scales exponentially, i.e., 2^N, with the number of qubits, N, we can expect the approximation to become very good with only a few qubits. In general, the protocol can be described by the following unitary operation:

$$\hat{U}[|\psi\rangle_{\mathrm{CV}}|\mathbf{0}\rangle_{\mathrm{DV}}] = \sqrt{(1-\varepsilon)}|\tilde{0}\rangle_{\mathrm{CV}}|\Psi\rangle_{\mathrm{DV}} + \sqrt{\varepsilon}|\Phi_\varepsilon\rangle_{\mathrm{CV/DV}}, \tag{1}$$

where $|\mathbf{0}\rangle_{\mathrm{DV}} = \otimes_{k=1}^{N}|0\rangle_k$ is the product of the ground states of the qubits, $|\Psi\rangle_{\mathrm{DV}}$ is the encoded DV state, and $|\Phi_\varepsilon\rangle_{\mathrm{CV/DV}}$ is a residual entangled CV-DV state defined to make $\hat{U}$ unitary and such that $\langle\Phi_\varepsilon|\tilde{0}\rangle = 0$. ε is a real parameter, $0 \le \varepsilon \le 1$, quantifying the error of the protocol, e.g., due to the CV-DV dimensionally mismatch. ε thus depends on the input state, and a successful protocol should aim to minimize ε for a large class of input states.

The input state can be recovered by applying $\hat{U}^\dagger$. If the CV mode is completely reset to the state $|\tilde{0}\rangle_{\mathrm{CV}}$ after the application of $\hat{U}$, the fidelity, F, between the input and recovered state is related to ε by

$$(1-\varepsilon)^2 \le F \le 1-\varepsilon, \tag{2}$$

with the exact value of F depending on the input state (details are given in the Supplemental Material [14]).

We now show how to decompose $\hat{U}$ into experimentally accessible two-mode interactions. A circuit diagram of the encoding unitary is shown in Fig. 1(b). It consists of N interaction terms, each of which are composed of two interactions, $\hat{V}_k$ and $\hat{W}_k$, between the CV mode and one of the qubits. These interactions are conditional displacements [8,15,16] that are generated by a Rabi-type Hamiltonian, i.e., a coupling between a quadrature operator of the CV mode and a Pauli operator of the qubit:

$$\hat{V}_k = \exp\left[i\frac{\pi}{2\lambda 2^k}\hat{q}\hat{\sigma}_y^{(k)}\right]$$
$$\hat{W}_k = \begin{cases} \exp\left[i\frac{\lambda 2^k}{2}\hat{p}\hat{\sigma}_x^{(k)}\right], & \text{if } k < N \\ \exp\left[-i\frac{\lambda 2^k}{2}\hat{p}\hat{\sigma}_x^{(k)}\right], & \text{if } k = N \end{cases}, \tag{3}$$

where $\hat{q}$ and $\hat{p}$ are the quadrature operators of the CV mode satisfying the commutation relation $[\hat{q},\hat{p}] = i$ and $\sigma_x^{(k)}$ and $\sigma_y^{(k)}$ are the Pauli-x and y operators of the kth qubit. The interaction parameter λ is the only free parameter of the protocol. As we show below, it should be optimized according to the number of qubits and the size of the input state, i.e., the wideness of the support of the input state in phase space. Importantly, a single value of λ can be used to encode a wide range of different CV states, meaning that little knowledge of the input CV state is required for the protocol to work. In the Supplemental Material [14], we show that the interactions defined in Eq. (3) achieves the desired unitary operation of Eq. (1) for arbitrary states, with ε decreasing with N. The qubit state after the interaction is

$$|\Psi\rangle_{\mathrm{DV}} \propto \sum_s \psi(q_s)|\phi\rangle_s, \tag{4}$$

where the sum is over 2^N terms, $|\phi_s\rangle$ form a specific orthonormal basis of the qubit space, ψ is the q-quadrature wave function of the input CV state, and q_s form an equidistant array of 2^N numbers from $-\lambda(2^N-1)$ to $\lambda(2^N-1)$ with spacing 2λ (see the Supplemental Material [14] for details). Thus, the qubit state samples the wave function at 2^N discrete points. From this feature we can intuitively understand how we should tune λ: First, to accurately capture variations in the CV wave function, the distance between the samples should be smaller than

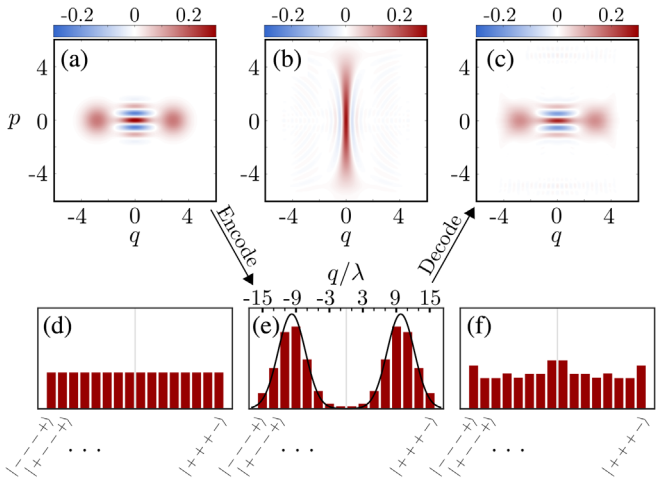

FIG. 2. Example of encoding and recovery of a CV Schrödinger's cat state, $(e^{-i\sqrt{2}\alpha\hat{p}} + e^{i\sqrt{2}\alpha\hat{p}})|\mathrm{vac}\rangle$ with $\alpha = 2$, using $N = 4$ qubits and $\lambda = 0.29$. Wigner functions (a)–(c) of the CV mode and probability distributions (d)–(f) of the qubits before encoding (a),(d), after encoding (b),(e), and after decoding (c),(f) with the CV mode completely reset to the state $|\tilde{0}\rangle_{\mathrm{CV}}$ after the encoding. The black curve in (e) shows the q-quadrature distribution of the input CV state with the x axis shown at the top of the figure.

any large variation of ψ, i.e., 2λ should be sufficiently small. Second, to capture the entire wave function, the sampling axis should be sufficiently wide, i.e., $\lambda(2^N - 1)$ should be large. Satisfying both of these constraints becomes easier for larger N, and for fixed N we can expect an optimum λ to exist.

The state $|\tilde{0}\rangle_{\mathrm{CV}}$ is given by

$$|\tilde{0}\rangle_{\mathrm{CV}} = \frac{1}{\sqrt{2\lambda}} \int dq \, \mathrm{sinc}\left(\pi \frac{q}{2\lambda}\right) |q\rangle, \tag{5}$$

where $\mathrm{sinc}(x) = \sin(x)/x$ and $|q\rangle$ denotes a $\hat{q}$ eigenstate, e.g., $\hat{q}|q\rangle = q|q\rangle$. To decode the CV state with the inverse unitary, $\hat{U}^\dagger$, the CV mode should first be prepared in the state $|\tilde{0}\rangle_{\mathrm{CV}}$. Since the encoding protocol approximately leaves the CV mode in state $|\tilde{0}\rangle_{\mathrm{CV}}$, this can be done by applying $\hat{U}$ to an arbitrary CV state, e.g., a vacuum or thermal state, along with ancillary qubits. In fact, to prepare $|\tilde{0}\rangle_{\mathrm{CV}}$ it suffices to use the same qubit for all N interactions by resetting the qubit to its ground state after each $\hat{W}\hat{V}$ interaction. Alternatively, $|\tilde{0}\rangle_{\mathrm{CV}}$ can be approximated with fidelity 0.89 by a squeezed vacuum state with squeezing parameter $\log(1.12/\lambda)$ (details in the Supplemental Material [14]). We note that the exact state $|\tilde{0}\rangle_{\mathrm{CV}}$ is in fact unphysical, as it has infinite energy since $\langle\tilde{0}|\hat{q}^2|\tilde{0}\rangle = \infty$ for all λ. However, finite energy states, e.g., the state prepared by applying $\hat{U}$ to vacuum, can approximate $|\tilde{0}\rangle_{\mathrm{CV}}$ with high fidelity.

An example of the encoding and recovery of a CV Schrödinger's cat state is shown in Fig. 2. Figure 2(e) shows how the input CV wave function is directly mapped onto the qubits (with a suitable qubit basis choice). Meanwhile, Fig. 2(b) shows how the CV mode approximately transforms to the state $|\tilde{0}\rangle_{\mathrm{CV}}$. The state shown in Fig. 2(c) is the recovered state after the CV mode is completely set to $|\tilde{0}\rangle_{\mathrm{CV}}$ and the qubits are decoded onto the CV mode, i.e., as shown in the circuit of Fig. 1(a). The small differences between Figs. 2(a) and 2(c) are due to the nonzero ε arising from the mapping. However, the key features of the CV state, such as the position of the coherent peaks and the central interference pattern with negative values, are preserved.

We now numerically demonstrate this result for specific input states. We first consider Fock states, as these represent fundamental quantum basis states, spanning the entire CV mode, with experimentally relevant quantum states typically having main support on low photon–number Fock states. Figure 3(a) shows how ε depends on λ for $N = 4$ and $N = 10$ qubits, respectively, using Fock

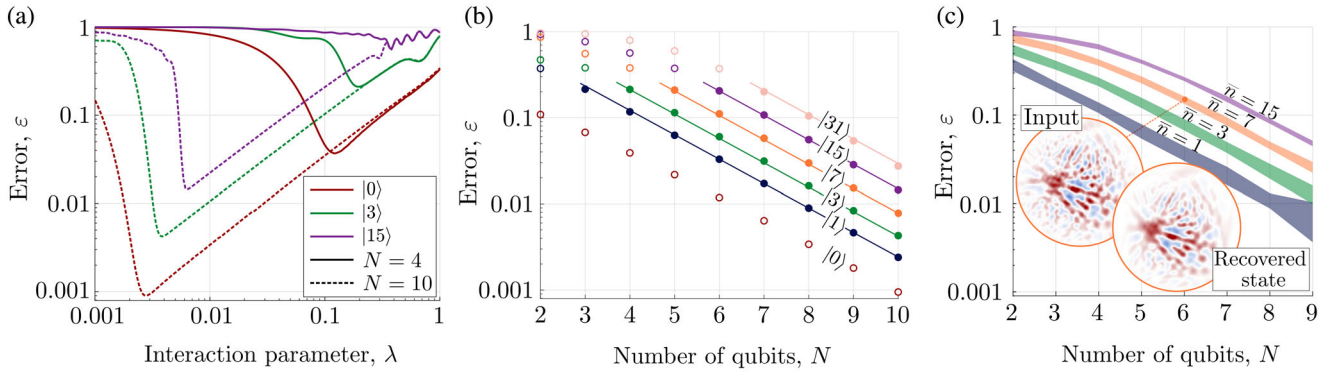

FIG. 3. (a) Error, ε, as a function of the interaction parameter λ for $N = 4$ and 10 qubits with Fock state inputs. (b) Error as a function of qubit number for Fock state inputs using the optimal λ for each state. Lines show a fit to $\varepsilon(N, n) = e^{-aN}(bn + c)$, using the values of the filled circles. (c) Error as a function of qubit number randomly sampled input states with different fixed mean photon number $\bar{n}$. The shaded areas contain states with ε within 1 standard deviation from the mean ε of the sample. The inserts show the Wigner function of an example input state with $\bar{n} = 7$ and the corresponding recovered state using $N = 6$ qubits.

states as inputs. For each input we find that there exists an optimum λ as expected, and that as we add more qubits, this optimum shifts to smaller values. We also find that, for any fixed λ, smaller number Fock states are better encoded than larger number Fock states. Thus, one setting optimized to encode large states can simultaneously be used to encode smaller states with as good or better performance.

Figure 3(b) shows how ε depends on the number of qubits for Fock state inputs, choosing the optimum λ for each point. We observe a clear exponential decrease in ε with increasing number of qubits. Additionally, fixing ε we find that adding a single qubit allows the storage of approximately twice as large input states, e.g., 4 qubits enable the encoding of $|1\rangle$ with $\varepsilon = 0.1$, while 5 qubits allow the encoding of $|3\rangle$ with the same error, 6 qubits can encode $|7\rangle$, and so on. This scaling is confirmed by the good agreement to the empirical equation for the error for Fock state n using N qubits, $\varepsilon(N, n) = e^{-aN}(bn + c)$, which is shown by the lines of Fig. 3(b) using the fitted values of $(a, b, c) = (0.65, 0.62, 1.04)$. The exponential scaling with the number of qubits and linear scaling with the Fock number shows that the protocol efficiently utilizes the dimensionality of the qubits, such that large CV states can be encoded using relatively few qubits.

To demonstrate the versatility of the protocol, Fig. 3(c) shows the performance for randomly sampled input states (see the Supplemental Material [14] for details on these states). A typical example of the Wigner function of a random state with $\bar{n} = 7$ photons is shown in the inset of Fig. 3(c). For each N and $\bar{n}$ in Fig. 3(c), we calculate ε for 100 of such random states using a single λ chosen to approximately optimize the average ε. The shaded area denotes the states within 1 standard deviation from the mean ε of the samples. As with the Fock states, we observe an exponential decrease in ε with N. In addition, we again note that adding a single qubit allows the encoding of states with approximately twice the mean photon number, keeping ε fixed.

Next, we check the stability of our scheme against errors occurring in the qubit system while the state is encoded. In particular, we consider the qubit dephasing channel

$$\Lambda_z(\rho) = \hat{K}_z^{(1)}\rho[\hat{K}_z^{(1)}]^\dagger + \hat{K}_z^{(2)}\rho[\hat{K}_z^{(2)}]^\dagger, \tag{6}$$

and qubit amplitude damping channel

$$\Lambda_\Gamma(\rho) = \hat{K}_\Gamma^{(1)}\rho[\hat{K}_\Gamma^{(1)}]^\dagger + \hat{K}_\Gamma^{(2)}\rho[\hat{K}_\Gamma^{(2)}]^\dagger, \tag{7}$$

with Kraus operators

$$\hat{K}_z^{(1)} = \sqrt{1 - p_z}\hat{I}, \qquad \hat{K}_z^{(2)} = \sqrt{p_z}\hat{\sigma}_z \tag{8}$$

$$\hat{K}_\Gamma^{(1)} = |0\rangle\langle 0| + \sqrt{1-\Gamma}|1\rangle\langle 1|, \qquad \hat{K}_\Gamma^{(2)} = \sqrt{\Gamma}|0\rangle\langle 1|, \tag{9}$$

where ρ denotes the qubit density matrix, p_z denotes the probability of a single-qubit phase flip, and Γ denotes the probability of a single qubit decay event. Figure 4(a) shows the fidelity of the recovered state after the CV mode is reset and each qubit has experienced either dephasing or amplitude damping for an input 5-photon Fock state, $|5\rangle$, and a random state with $\bar{n} = 3$ average photons, $|\psi_{\text{ran}}\rangle$ using $N = 6$ qubits. As can be expected, the fidelity drops as the qubits experience more noise. However, a single figure of merit, such as the fidelity, is often insufficient to capture the full nonclassical aspects of non-Gaussian CV states. Therefore, we also qualitatively analyze the Wigner functions, quadrature distributions, and photon distributions of the two selected non-Gaussian trial states. Other input states have shown similar behavior. Figures 4(c) and 4(d) show the recovered states after each

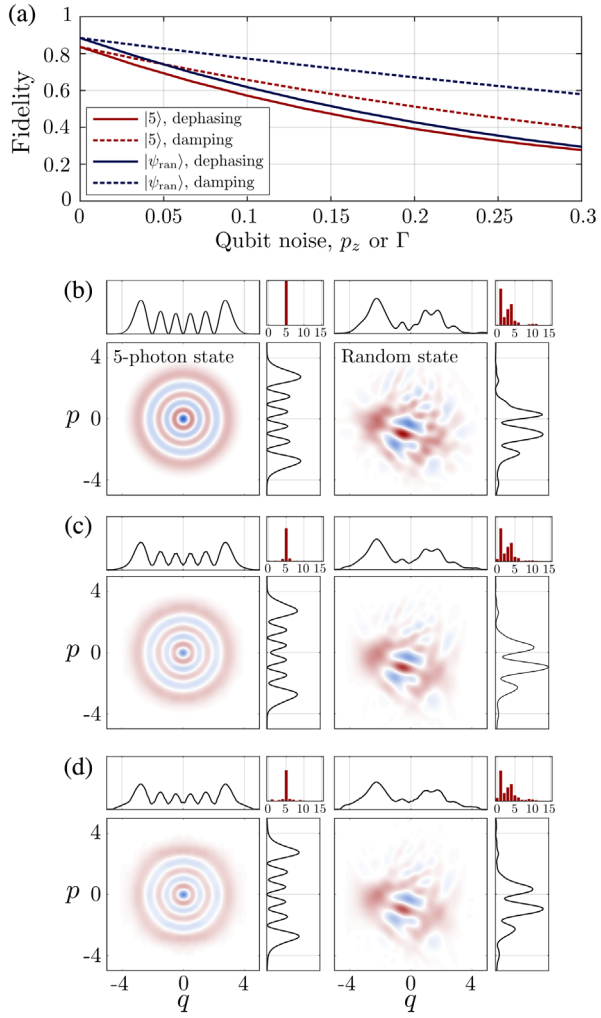

FIG. 4. (a) Fidelity of recovered states when the qubits undergo dephasing or amplitude damping for an input 5-photon Fock state, and a random state with $\bar{n} = 3$ using $\lambda = 0.07$ and $N = 6$ qubits. (b)–(d) Wigner functions, quadrature distributions, and photon number distributions for the 5-photon Fock state (left) and the $\bar{n} = 3$ photon random state (right). (b) Input states. (c) Output when each qubit undergoes dephasing with $p_z = 0.05$. (d) Output when each qubit undergoes amplitude damping with $\Gamma = 0.05$.

qubit has undergone dephasing or amplitude damping with an error probability of $p_z = 0.05$ or $\Gamma = 0.05$. For both channels we observe a smearing of the q-quadrature distributions while the p-quadrature distributions remain almost intact compared to the input for both trial states. More importantly, we find that the negative regions of the Wigner functions (highlighted in blue), which are strong indicators of nonclassicality, remain non-negligible. Thus, even moderate error rates do not have a severe effect on the recovered states.

Another important noise source is noise occurring during the encoding and decoding operations. In the Supplemental Material [14], we analyze this type of noise using a master equation approach. For such noise, adding more qubits can eventually degrade the performance of the protocol, since the encoding and recovery operations take longer to perform, thus accumulating more noise. To mitigate this, the conditional displacements should ideally be implemented on a timescale much faster than the noise rates.

In conclusion, we have presented a feasible unitary protocol to map arbitrary CV states into a few qubits. This can be realized using only conditional displacements generated by Rabi-type coupling Hamiltonians, which currently are available in trapped-ion systems [16] and superconducting circuits [8]. The protocol is fully deterministic and requires no measurements or feed-forward. The error rates caused by the finite dimensionality of the qubit subsystem decrease exponentially with the number of qubits. Furthermore, small dephasing or amplitude-damping errors acting on the qubits do not translate into large errors in the protocol. We have focused on encoding arbitrary CV states into qubits, but similar techniques might be used to map arbitrary multiqubit states into a single CV mode. Such mapping could facilitate multiqubit operations and hardware-efficient qubit transfers. We leave this as an interesting open direction for future work.

This project was supported by the Danish National Research Foundation through the Center of Excellence for Macroscopic Quantum States (bigQ, DNRF0142). R. F. and K. P. acknowledge Project No. 21-13265X of the Czech Science Foundation. This project has received funding from the European Union's 2020 research and innovation programme (CSA - Coordination and support action, H2020-WIDESPREAD-2020-5) under Grant Agreement No. 951737 (NONGAUSS). J. B. B. acknowledges support from the Independent Research Fund Denmark.

*Corresponding author.
jhast@fysik.dtu.dk

[1] C. Weedbrook, S. Pirandola, R. García-Patrón, N. J. Cerf, T. C. Ralph, J. H. Shapiro, and S. Lloyd, Gaussian quantum information, Rev. Mod. Phys. **84**, 621 (2012).

[2] F. Arute, K. Arya, R. Babbush, D. Bacon, J. C. Bardin, R. Barends, R. Biswas, S. Boixo, F. G. S. L. Brandao, D. A. Buell *et al.*, Quantum supremacy using a programmable superconducting processor, Nature (London) **574**, 505–510 (2019).

[3] J.-i. Yoshikawa, S. Yokoyama, T. Kaji, C. Sornphiphatphong, Y. Shiozawa, K. Makino, and A. Furusawa, Generation of one-million-mode continuous-variable cluster state by unlimited time-domain multiplexing, APL Photonics **1**, 060801 (2016).

[4] W. Asavanant, Y. Shiozawa, S. Yokoyama, B. Charoensombutamon, H. Emura, R. N. Alexander, S. Takeda, J.-i. Yoshikawa, N. C. Menicucci, H. Yonezawa *et al.*, Generation of time-domain-multiplexed two-dimensional cluster state, Science **366**, 373 (2019).

[5] M. V. Larsen, X. Guo, C. R. Breum, J. S. Neergaard-Nielsen, and U. L. Andersen, Deterministic generation of a two-dimensional cluster state, Science **366**, 369 (2019).

[6] N. Ofek, A. Petrenko, R. Heeres, P. Reinhold, Z. Leghtas, B. Vlastakis, Y. Liu, L. Frunzio, S. M. Girvin, L. Jiang *et al.*, Extending the lifetime of a quantum bit with error correction in superconducting circuits, Nature (London) **536**, 441 (2016).

[7] L. Hu, Y. Ma, W. Cai, X. Mu, Y. Xu, W. Wang, Y. Wu, H. Wang, Y. P. Song, C.-L. Zou *et al.*, Quantum error correction and universal gate set operation on a binomial bosonic logical qubit, Nat. Phys. **15**, 503 (2019).

[8] P. Campagne-Ibarcq, A. Eickbusch, S. Touzard, E. Zalys-Geller, N. E. Frattini, V. V. Sivak, P. Reinhold, S. Puri, S. Shankar, R. J. Schoelkopf *et al.*, Quantum error correction of a qubit encoded in grid states of an oscillator, Nature (London) **584**, 368 (2020).

[9] B. de Neeve, T. L. Nguyen, T. Behrle, and J. Home, Error correction of a logical grid state qubit by dissipative pumping, Nat. Phys. (2022).

[10] C. D. Bruzewicz, J. Chiaverini, R. McConnell, and J. M. Sage, Trapped-ion quantum computing: Progress and challenges, Appl. Phys. Rev. **6**, 021314 (2019).

[11] P. Krantz, M. Kjaergaard, F. Yan, T. P. Orlando, S. Gustavsson, and W. D. Oliver, A quantum engineer's guide to superconducting qubits, Appl. Phys. Rev. **6**, 021318 (2019).

[12] J. Fiurášek, Encoding the quantum state of cavity mode into an atomic beam, Phys. Rev. A **66**, 015801 (2002).

[13] X.-y. Chen, L. Han, and L.-z. Jiang, Quantum state conversion between continuous variable and qubits systems, Phys. Lett. A **359**, 587 (2006).

[14] See Supplemental Material at http://link.aps.org/supplemental/10.1103/PhysRevLett.128.110503 for a derivation of Eq. (2), an analytical analysis of the protocol, details on the state $|\tilde{0}\rangle_{\mathrm{CV}}$, elaboration on the random states used, and master equation simulations.

[15] P. C. Haljan, K.-A. Brickman, L. Deslauriers, P. J. Lee, and C. Monroe, Spin-Dependent Forces on Trapped Ions for Phase-Stable Quantum Gates and Entangled States of Spin and Motion, Phys. Rev. Lett. **94**, 153602 (2005).

[16] C. Flühmann, V. Negnevitsky, M. Marinelli, and J. P. Home, Sequential Modular Position and Momentum Measurements of a Trapped Ion Mechanical Oscillator, Phys. Rev. X **8**, 021001 (2018).